Desalination 567 (2023) 116927

Contents lists available at ScienceDirect

Desalination

journal homepage: www.elsevier.com/locate/desal

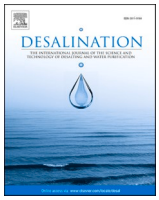

A systematic non-equilibrium thermodynamics approach for assessing transport mechanisms in membrane distillation

Kim R. Kristiansen, Øivind Wilhelmsen, Signe Kjelstrup *

PoreLab, Department of Chemistry, Norwegian University of Science and Technology, 7491 Trondheim, Norway

HIGHLIGHTS

- A systematic NET approach for analysis of transport mechanisms in MD is presented.
- Commonly employed membrane distillation formulae shown to be special cases of the NET approach.
- Temperature difference is the true driving force in direct-contact membrane distillation.
- Influence of membrane surface wetting state elucidated.
- Incorporation of sorption effects in nano-scale pores demonstrated

ARTICLE INFO

Keywords:
Membrane distillation
Non-equilibrium thermodynamics
Coupled transport
Boundary driven transport
Interface transport
Hydrophobic membrane

ABSTRACT

Membrane distillation (MD) is a promising technique for purifying volatile liquids at temperatures below their boiling points. This study presents a systematic non-equilibrium thermodynamics (NET) approach for analysis of transport mechanisms in direct-contact membrane distillation (DCMD). By incorporating the transport properties of the membrane, membrane interfaces, and temperature polarization layers, a unified framework is established to assess mass and heat transfer, including coupling effects in the composite membrane system. Explicit expressions for the transport properties are derived, and a numerical solution procedure is used to obtain temperature and partial pressure profiles through the system. The NET approach reveals that the temperature difference across the membrane is the true driving force of mass transfer, which after suitable approximations is equivalent to the saturation pressure difference. The commonly employed formula for distillate flux in MD literature was found to agree with the comprehensive NET approach within 3% when predicting the water flux through a DuraPore GVHP membrane. Incorporating a correction factor that accounts for kinetic heat-mass coupling effects improves the agreement to 0.5%. The simplified model disregards interfacial transport phenomena and mass-heat coupling. These effects are shown to be insignificant for the DuraPore GVHP membrane. However, it is crucial to account for temperature polarization to obtain agreement with experimental results. The resistance of the vapor-liquid interface is shown to be more important if the membrane has a Cassie-Baxter wetting state than a Wenzel wetting state, and this can enhance the water flux. When the pore-sizes approach the nanometer scale, we show that direct interactions between the molecules and the pore walls must be accounted for due to sorption effects. In applications where nanometer scale pores are important, such as in systems where the membrane must maintain a large pressure difference, it may be important to take such corrections into consideration. The presented NET approach provides a comprehensive toolkit for assessing and analyzing transport properties in membrane systems, which can be used to better understand how the properties of MD systems can be tailored to enhance performance.

* Corresponding author.
E-mail address: signe.kjelstrup@ntnu.no (S. Kjelstrup).

https://doi.org/10.1016/j.desal.2023.116927
Received 11 June 2023; Received in revised form 11 August 2023; Accepted 15 August 2023
Available online 24 August 2023

1. Introduction

Membrane distillation (MD) is used as an umbrella term for processes that utilize membranes as transport media to facilitate distillation of volatile components at operating temperatures generally below the boiling point of either component at the given conditions. Research into the advancement of such processes is timely, given the steadily increasing problems of energy dissipation by waste heat, assessed in e.g. [1], and the general scarcity of potable water, which has been a major concern for decades [2]. Membrane distillation can help solve both problems at the same time, by utilizing the waste heat or thermal energy to produce potable water.

The general MD processes and their applications are described in detail by Khayet and Matsuura [3], and in several recent reviews [4–6]. These reviews document a bustling research activity and advances in relevant techniques and technologies. The theoretical models describing the physical mechanisms of transport, however, are routinely over-simplified. For instance, interfacial transport phenomena are usually neglected, even though works such as that of Villaluenga and Kjelstrup highlight the importance of the interfacial thermal resistance [7]. Addition of resistances is also typically justified by an electrical resistance analogy, which is how relations such as the Bosanquet formula are often interpreted [3]. This analogy is not so straightforward when transport phenomena are coupled, and addition rules should be thoroughly justified on the grounds of physical conservation laws [8]. The common approximations used in the MD literature may therefore miss out on key mechanisms that may help direct research towards improvement of membrane materials and modules.

In order to help rectify this issue, we present in this work a detailed non-equilibrium thermodynamics approach to the problem and provide a robust addition rule for the resistances of the coupled heterogeneous system. By use of this approach, the approximations commonly applied in the literature can be properly justified from numerical computation and can also provide a range of validity for such approximations. When considering systems that are beyond this range of validity, such an approach may help to shed light on mechanisms that can be exploited for the improvement of the MD processes. The purpose of this work is to provide a method that can be used to assess details that are neglected in commonly used models, such as the effects of interfacial transport phenomena, the effects of pore size variance and other non-linear effects.

In previous works on MD, such as that of Schofield et al. [9], it was concluded that the properties of the membrane itself are not as important as the design of the process modules. However, more recent experimental work by Kuipers et al. [10] on a non-isobaric variant of the direct-contact membrane distillation (DCMD) process stresses the need for membranes that can withstand high transmembrane pressure differences without allowing liquid to leak through and still maintain high distillation performance, as pointed out by various authors [11–15]. The simulation work by Rauter et al. [16] demonstrated the importance of the wetting state of the liquid-membrane interface. This work highlights a largely unexplored avenue of MD research and development, and a model that includes interfacial transport phenomena like the one developed in this work, helps to shed light on the effects of and mechanisms with which the interfacial wetting state influences the performance of the MD process. As the need for more specialized membranes with more extreme properties rises to meet the demands of processes such as non-isobaric DCMD, the tools provided in this work can be used to properly assess the effects of superhydrophobic membrane surfaces or nanoscale pore sizes on transport phenomena as well as efficiency.

We begin in Section 2 by introducing the transport properties that are identified through well-defined experiments on the heterogeneous membrane system sketched in Fig. 1. We next show how these properties relate to the generalized resistances R_{ij}^{tot}, which satisfy a convenient addition rule due to conservation of energy and mass. This addition rule allows us to decompose the resistances into contributions from the subsystems to the total system. In Section 3, we show how to exploit the properties of the generalized resistances to construct the transport properties of the heterogeneous system from the local transport properties of each individual subsystem, which relate to the structural and chemical properties of the membrane. Results are presented in Section 4 and concluding remarks are provided in Section 5.

2. The overall transport process

Although the methodology employed here is general and can be applied to any variant of MD, we will focus specifically on DCMD. We consider first the prototypical DCMD system illustrated in Fig. 1, where we control the state of the liquid phases in domains Γ_1 and Γ_2. The purpose of Sections 2–3 is to systematically develop a complete model for the governing equations for transport of energy and matter through

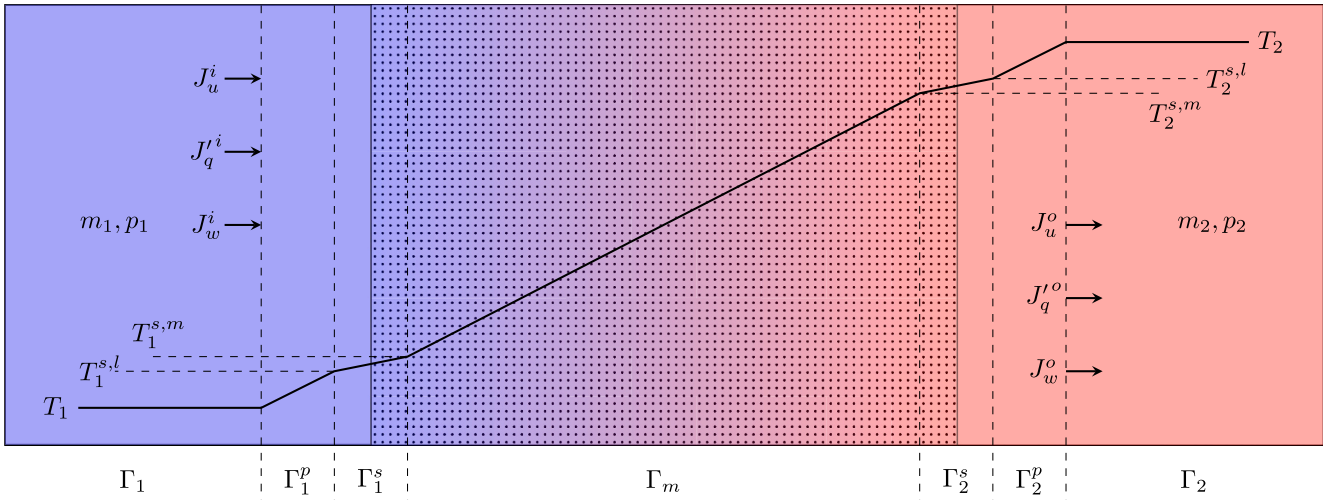

Fig. 1. Illustration of the DCMD membrane system, partitioned into the bulk liquid regions Γ_1 and Γ_2, the polarization layers Γ_1^p and Γ_2^p, the liquid-membrane interfaces Γ_1^s and Γ_2^s, and the bulk membrane Γ_m. The liquid phases are characterized by the molality m, the pressure p, and the temperature T. In response to differences in these quantities, there will be fluxes of energy and mass, J_u and J_w, into and out of the membrane system. Also indicated is the measurable heat flux J'_q, which depends on the other two fluxes. An example temperature profile has been included, with the positions of the temperatures $T_i^{s,l}$ and $T_i^{s,m}$ in the boundary regions shown. The regions are not drawn to scale and are presented as such for ease of illustration.

this system with a basis in non-equilibrium thermodynamics. We start by summarizing the governing assumptions.

The membrane is filled with a vapor-air mixture. We neglect the net transport of air through the membrane, on account of low solubility in the adjoining liquid phases. This precludes any viscous flow of gaseous mixture through the membrane. Experiments are usually carried out under steady-state conditions, so the model is also formulated at these conditions. There is no net accumulation of energy or mass anywhere in the system, and the laws of energy and mass conservation give a constant energy flux, J_u, and water flux, J_w [17]. The reason for this choice of flux variables is that their spatial invariance provides a simple addition rule for the resistivities along the axis of transport. The excess entropy production σ_{tot} of the system can be written on discrete form [8]:

$$\sigma_{\text{tot}} = J_u \Delta_{1,2}\frac{1}{T} - J_w \Delta_{1,2}\frac{\mu_w}{T}, \tag{1}$$

where μ is the chemical potential and subscript w denotes water, T is the absolute temperature, and $\Delta_{n,k}f$ is shorthand for the difference $f_k - f_n$ for any scalar quantity f. This bilinear form of the entropy production identifies the driving forces $\Delta_{1,2}(1/T)$ and $-\Delta_{1,2}(\mu_w/T)$ as *conjugate* to the fluxes J_u and J_w, respectively. The driving forces are expressed to linear order in these fluxes as

$$\begin{aligned}\Delta_{1,2}\frac{1}{T} &= R^{\text{tot}}_{uu}J_u + R^{\text{tot}}_{um}J_w,\\ -\Delta_{1,2}\frac{\mu_w}{T} &= R^{\text{tot}}_{mu}J_u + R^{\text{tot}}_{mm}J_w.\end{aligned} \tag{2}$$

Onsager's famous theorem states that, $R^{\text{tot}}_{um} = R^{\text{tot}}_{mu}$, where R^{tot}_{ij} are the overall resistances per unit area. The terms resistivity and conductivity refer to intensive material properties, whereas the terms resistance and conductance refer to extensive properties that depend on geometrical properties such as thickness. We will use the convention that resistivities and conductivities are represented by lowercase symbols, and resistances and conductances are represented by uppercase symbols.

To obtain a more practical set of equations, we rewrite the chemical driving force in terms of differences in pressure, p, and composition [17], and rewrite Eq. 2 to

$$\begin{aligned}J'^{o}_q &= -\Lambda_{\text{tot}}\Delta_{1,2}T + q^{*o}J_w,\\ J_w &= -D_T\Delta_{1,2}T - L_p\left[\Delta_{1,2}p - \Pi\Delta_{1,2}m\right],\end{aligned} \tag{3}$$

where J'^{o}_q is the flux of measurable heat from the membrane system into Γ_2, Λ_{tot} is the overall thermal conductance, q^{*o} is the heat of transfer, D_T is the thermo-osmotic coefficient, m is the molality, Π is the molal osmotic pressure coefficient and the coefficient L_p relates to how the water flux depends on the pressure difference across the membrane. The measurable transport properties in Eq. 3 are defined as

$$\begin{aligned}\Lambda_{\text{tot}} &= -\left(\frac{J'^{o}_q}{\Delta_{1,2}T}\right)_{J_w=0} = \frac{1}{T_1T_2R^{\text{tot}}_{uu}},\\ q^{*o} &= \left(\frac{J'^{o}_q}{J_w}\right)_{\Delta_{1,2}T=0} = -\frac{R^{\text{tot}}_{um}}{R^{\text{tot}}_{uu}} - H_{w,2} = Q^*_{\text{tot}} - H_{w,2},\\ L_p &= -\left(\frac{J_w}{\Delta_{1,2}p}\right)_{\Delta_{1,2}T=0} = \frac{V_w}{T_1}\left(R^{\text{tot}}_{mm} - \frac{R^{\text{tot}}_{um}R^{\text{tot}}_{mu}}{R^{\text{tot}}_{uu}}\right)^{-1},\\ D_T &= -\left(\frac{J_w}{\Delta_{1,2}T}\right)_{\Delta_{1,2}\mu_{T,w}=0} = \frac{q^{*o}L_p}{V_wT_2},\end{aligned} \tag{4}$$

where Q^*_{tot} is the energy of transfer, V_w is the partial molar volume of liquid water, and $H_{w,2}$ is the partial molar enthalpy of the liquid water in Γ_2. The molal osmotic pressure coefficient is

$$\Pi = \left(\frac{\Delta_{1,2}p}{\Delta_{1,2}m}\right)_{J_w=0,\Delta_{1,2}T=0} = \frac{\nu RT_1M_w\Gamma_s}{V_w}. \tag{5}$$

where R is the universal gas constant, M_w the molar mass of water, and Γ_s and ν are respectively the thermodynamic factor and the van't Hoff factor of the dissolved salt. In a gaseous medium, it is more common to express the mass transfer resistance in terms of a diffusivity D. Since we will be dealing with a gaseous phase in the bulk membrane, it will be convenient to relate the permeability to an effective diffusivity, D_{tot}, as follows

$$D_{\text{tot}} = \frac{R^2T^2L_p\delta}{V_wp_w} \tag{6}$$

where p_w is the partial pressure of water in the gas phase, and δ is the membrane thickness. We will show how such a relation comes naturally from our approach.

Many of the quantities in the above equations are measurable quantities. The thermal conductance, Λ_{tot}, is obtained by measuring the outgoing heat flux resulting from a temperature difference when the net migration of water stops. The heat of transfer, q^{*o}, is obtained by measuring the outgoing heat flux when there is no temperature difference. The thermo-osmotic coefficient D_T can be measured directly by measuring the net flux of water across the system due to a temperature difference when $\Delta_{1,2}p = \Pi\Delta_{1,2}m$ (or, trivially, when they are both zero), and L_p is measured by recording the water flux when either applying a pressure difference when there is no difference in temperature and composition, or measured as $L_p\Pi$ by recording the osmotic flux that results from the composition difference at isothermal and isobaric conditions.

We have chosen the force-flux formulation with constant fluxes J_u and J_w, because the total resistances R^{tot}_{ij} can be decomposed into additive contributions, one from each subdomain Γ^p_1, Γ^s_1, Γ^p_2, Γ^s_2, and Γ_m. Following again the procedure explained in Ref. [8] for each subdomain, we then obtain

$$R^{\text{tot}}_{ij} = R^{p,1}_{ij} + R^{s,1}_{ij} + R^{p,2}_{ij} + R^{s,2}_{ij} + \delta\bar{r}^{m}_{ij} \tag{7}$$

where $R^{s,1}_{ij}$ and $R^{s,2}_{ij}$ are the interfacial resistances across the subdomains Γ^s_1 and Γ^s_2; $R^{p,1}_{ij}$ and $R^{p,2}_{ij}$ the resistances across the polarization layers Γ^p_1 and Γ^p_2; $\bar{r}^{m}_{ij}$ is the average resistivity of the bulk membrane, Γ_m, and δ is the thickness of the membrane. This simple addition rule applies to the resistances in Eq. (2) because of the spatial invariance of J_u and J_w. The measurable transport properties of Eq. (3) can thus be related to the set of total overall resistances in Eq. (2). We proceed to formulate the resistivities of each subsystem separately. We note that the local resistivities are always on the form

$$\begin{aligned}r^x_{uu} &= \frac{1}{T^2\lambda_x}\\ r^x_{um} &= r^x_{mu} = -\frac{Q^*_x}{T^2\lambda_x}\\ r^x_{mm} &= \frac{R^2T}{p_wD_x} + \frac{Q^{*2}_x}{T^2\lambda_x}\end{aligned} \tag{8}$$

where λ_x, Q^*_x, and D_x are the thermal conductivity, energy of transfer, and the diffusivity of the transport regime denoted x. The quantities λ_x and D_x are in principle measurable, as is the heat of transfer $q^*_x = Q^*_x - H_w$. When these quantities are obtained, the Onsager resistivities r^x_{ij} that are needed in Eq. (7) are identified using Eq. (8). It is also useful to invert the flux-force relations so that the fluxes are expressed as linear combinations of the driving forces. This requires an inversion of the resistivity matrix, which gives the conductivity matrix with elements

$$\ell^x_{uu} = T^2\lambda_x + Q^{*2}_x \frac{p_w D_x}{R^2 T}$$
$$\ell^x_{um} = \ell^x_{mu} = Q^*_x \frac{p_w D_x}{R^2 T} \tag{9}$$
$$\ell^x_{mm} = \frac{p_w D_x}{R^2 T}$$

3. Constructing the transport coefficients

3.1. The membrane bulk resistivities

In this section, we build a model for the bulk membrane in order to relate the local resistivities r^m_{ij} to the structural and chemical properties of the membrane. To construct the model for the bulk membrane, we consider transport through one single cylindrical pore in Section 3.1.1. This gives the resistivities r^c_{ij} of a single pore. We next use the cylindrical single pore model to construct the membrane bulk resistivities r^m_{ij} in Section 3.1.2.

3.1.1. Transport in a single pore

In this section, we seek the transport coefficients of a single pore that are needed to construct the transport coefficients of the membrane bulk cross section in Section 3.1.2. The pore diffusion coefficient is often calculated from the bulk interdiffusion coefficient D_h and the Knudsen diffusivity D_K by means of the Bosanquet formula [3]

$$\frac{1}{D_c} = \frac{1}{D_h} + \frac{1}{D_\mathrm{K}} \tag{10}$$

which was first introduced by Bosanquet [18], justified by kinetic theory [19], and thoroughly tested with molecular dynamics simulations by Krishna et al. [20]. Given that the membrane thickness δ is much larger than the average pore radius $\bar{a}$, we find it reasonable to use the arguments leading up to Eq. (10) in the limit of an infinitely long pore to what will henceforth be referred to as the *generalized Bosanquet formula*

$$r^c_{ij} = r^\mathrm{K}_{ij} + r^h_{ij}, \tag{11}$$

where the superscripts K and h refer to the limits Kn→∞ and Kn→0, respectively, where Kn is the Knudsen number. The energy-mass transport coefficients in the limit Kn→∞ in a hydrophobic cylinder were discussed in detail in Ref. [21]. We denote the quantities D_K, λ_K and Q^*_K the diffusivity, thermal conductivity and energy of transfer in the limit Kn→∞, which is thoroughly discussed in Ref. [21]. The equivalent quantities in the limit Kn→0, D_h, λ_h and Q^*_h, are the transport properties of the bulk water-air mixture. We give explicit expressions for all these quantities in Appendix C. Based on the addition rule in Eq. (11), we can identify the following quantities for the cylindrical pore (subscript c)

$$\lambda_c = \frac{\lambda_\mathrm{K}\lambda_h}{\lambda_\mathrm{K}+\lambda_h},$$
$$Q^*_c = \frac{\lambda_\mathrm{K} q^*_h + \lambda_h q^*_\mathrm{K}}{\lambda_\mathrm{K}+\lambda_h} + H_{w,g}, \tag{12}$$
$$D_c = \left(\frac{1}{D_h} + \frac{1}{D_\mathrm{K}} + \frac{p_w}{T(\lambda_\mathrm{K}+\lambda_h)}\left(\frac{q^*_h - q^*_\mathrm{K}}{RT}\right)^2\right)^{-1},$$

which, as the notation implies, are the effective thermal conductivity λ_c, energy of transfer Q^*_c and diffusion coefficient D_c of the pore with the combined transport modes. The local energy of transfer in the gas phase includes the partial molar enthalpy $H_{w,g}$ of water in the gas phase. We see in particular that the expression for the diffusion coefficient differs from the original Bosanquet formula in Eq. (10) by the addition of an extra mass transfer resistance related to the heat-mass coupling of the two transport modes. This term is negligible in both limits, but provides a significant but small correction in the transition regime.

3.1.2. Transport across the bulk membrane

We model the membrane cross section as a solid material perforated by cylindrical pores. A given surface element of the membrane covers several such pores in addition to solid material. This is a crucial point: In order to add flux contributions from each individual pore, the flux-force relations on the form of Eq. (2) must be inverted. The surface-averaged conductivities ℓ^m_{ij} of a given portion of the membrane surface area A are obtained by adding the conductivities of all pores in the cross section, along with the conductivity of the solid material, and dividing by the surface area A. This gives the bulk conductivities

$$\ell^m_{ij} = \frac{1}{A}\sum_k \pi a_k^2 \ell^c_{ij,k} + \frac{A_s}{A}\ell^s_{ij}, \tag{13}$$

where A_s is the total area of the solid material, ℓ^s_{ij} the conductivity of the solid material, and the sum is taken over all pores covered by the area. We assume that the solid material is impermeable to mass transfer, such that $\ell^s_{um} = \ell^s_{mu} = 0$, $\ell^s_{mm} = 0$, and $\ell^s_{uu} = T^2\lambda_s$ with λ_s being the effective thermal conductivity of the solid matrix. Given that the area, A, covers a representative sample of pores, we can replace the sum over pores by the total number N_p of pores times the integral over the pore size distribution $F(a)$

$$\sum_k \pi a_k^2 \ell^c_{ij,k} = \pi N_p \int_{\Gamma_p} \mathrm{d}a \ell^c_{ij}(a) a^2 F(a) = \pi N_p \left\langle a^2 \ell^c_{ij} \right\rangle. \tag{14}$$

The average pore cross-sectional area is $A_p = N_p \pi \langle a^2 \rangle$, where a is the pore radius. We define the correction factors $\mathscr{K}_{\sigma,ij}$ such that

$$\sum_k \pi a_k^2 \ell^c_{ij,k} = A_p \ell^c_{ij}(\bar{a}) \frac{\left\langle a^2 \ell^c_{ij} \right\rangle}{\langle a^2 \rangle \ell^c_{ij}(\bar{a})} = A_p \ell^c_{ij}(\bar{a}) \mathscr{K}_{\sigma,ij}, \tag{15}$$

where $\bar{a}$ is the mean pore radius. The surface porosity is $\phi_s = A_p/A$. Then since $A_p + A_s = A$, we have $A_s/A = 1 - \phi_s$. We obtain the bulk conductivities

$$\ell^m_{uu} = \phi_s \left[T^2\lambda_c(\bar{a}) + Q^{*2}_c(\bar{a}) \frac{p_w}{R^2 T} D_c(\bar{a})\right] \mathscr{K}_{\sigma,uu} + (1-\phi_s) T^2 \lambda_s,$$
$$\ell^m_{um} = \ell^b_{mu} = \phi_s Q^*_c(\bar{a}) \frac{p_w D_c(\bar{a})}{R^2 T} \mathscr{K}_{\sigma,um}, \tag{16}$$
$$\ell^m_{mm} = \frac{\phi_s p_w D_c(\bar{a})}{R^2 T} \mathscr{K}_{\sigma,mm}.$$

We can now obtain the local resistivities of the membrane bulk by inverting the matrix of conductivities. The total resistances of the membrane bulk are then obtained by integrating the local resistivities, which in general vary along the path of integration due to gradients in temperature and composition. In order to account for the fact that real pores are not straight cylinders, we introduce the tortuosity factor τ_p such that the effective average path length is $\tau_p \delta$. This factor has been firmly established in the literature [3]. The membrane bulk quantities are then the bulk thermal conductivity

$$\lambda_m = \frac{\phi_s}{\tau_p} \mathscr{K}_{\sigma,uu} \lambda_c(\bar{a}) + (1-\phi_s)\lambda_s + \frac{\phi_s Q^{*2}_c(\bar{a}) p_w D_c(\bar{a})}{\tau_p R^2 T^3} \left(\mathscr{K}_{\sigma,uu} - \frac{\mathscr{K}^2_{\sigma,um}}{\mathscr{K}_{\sigma,mm}}\right) \tag{17}$$

the bulk energy of transfer

$$Q^*_m = Q^*_c(\bar{a}) \frac{\mathscr{K}_{\sigma,um}}{\mathscr{K}_{\sigma,mm}} \tag{18}$$

and the bulk diffusion coefficient

$$D_m = \frac{\phi_s D_c(\bar{a})}{\tau_p} \mathscr{K}_{\sigma,mm}. \tag{19}$$

The local resistivities depend on the actual thermodynamic state of

the local representative elementary volume. The averaging procedure over the bulk membrane must typically be performed numerically with an initial guess of the values of the thermodynamic state variables across the system, and then iterated to the desired accuracy. We describe the systematic approach to this in Appendix B. From this point on, we operate in the theory with an adequate initial guess: if the resistivities are constant through the membrane, then it follows from the conservation laws that the gradients in the inverse temperature and the ratio μ/T are constant. Evaluating the resistivities at the arithmetic mean values of these state variables is roughly equivalent to evaluating them at the arithmetic mean temperature $\bar{T}$ and geometric mean partial pressure $\widehat{p}$. Assuming that the vapor is saturated inside the membrane, the latter is approximately equal to the water saturation pressure evaluated at the mean temperature, $p_w^{\mathrm{sat}}(\bar{T})$. By these assumptions, the profiles of $\ln p_w$ and T are nearly odd functions over the domain, and thus the first order corrections to evaluating the coefficients at these values vanish, making this a good initial guess. To compute the resistivities, we use

$$\begin{aligned} r_{uu}^{\bar{m}} &= \frac{1}{\bar{T}^2\lambda_m}, \\ r_{um}^{\bar{m}} = r_{mu}^{\bar{m}} &= -\frac{Q_m^*}{\bar{T}^2\lambda_m}, \\ r_{mm}^{\bar{m}} &= \frac{R^2\bar{T}}{p_w^{\mathrm{sat}}(\bar{T})D_m} + \frac{Q_m^{*\,2}}{\bar{T}^2\lambda_m}, \end{aligned} \tag{20}$$

where D_m, Q_m^* and λ_m are evaluated at $\bar{T}$ and $p_w^{\mathrm{sat}}(\bar{T})$.

3.2. The liquid-membrane interfaces

The interface between the liquid phase and the bulk membrane is complicated, because the surface of a polymeric membrane is rough on the length scale of the pore size. The surface roughness is often the origin of the membrane hydrophobic qualities, see Wenzel [22] and Cassie and Baxter [23]. The transport properties of the pure water liquid-vapor interface were thoroughly investigated in Refs. [24, 25], referring to the following discrete formulation

$$\begin{aligned} \Delta_{l,g}\frac{1}{T} &= R_{qq}^{\mathrm{gl}} J_q^{\,g} + R_{q\mu}^{\mathrm{gl}} J_w \\ -\frac{1}{T^l}\Delta_{l,g}\mu_w\left(T^l\right) &= R_{\mu q}^{\mathrm{gl}} J_q^{\,g} + R_{\mu\mu}^{\mathrm{gl}} J_w \end{aligned} \tag{21}$$

where J_q^g is the measurable heat flux from the interface into the vapor phase. All resistances are positive and decay exponentially with temperature, and we present a numerical fit in Appendix C. Transforming to the set containing the energy flux J_u gives the following expressions for the resistivities that satisfy the addition rule in Eq. (7)

$$\begin{aligned} R_{uu}^{\mathrm{gl}} &= R_{qq}^{\mathrm{gl}}, \\ R_{um}^{\mathrm{gl}} = R_{mu}^{\mathrm{gl}} &= R_{q\mu}^{\mathrm{gl}} - H_{w,g}R_{qq}^{\mathrm{gl}}, \\ R_{mm}^{\mathrm{gl}} &= R_{\mu\mu}^{\mathrm{gl}} - 2H_{w,g}R_{q\mu}^{\mathrm{gl}} + H_{w,g}^2 R_{qq}^{\mathrm{gl}}. \end{aligned} \tag{22}$$

The available surface area of the vapor-liquid interface depends on the wetting state of the membrane surface. We distinguish between two states: the Wenzel (W) and the Cassie-Baxter (CB) state. In the former, the liquid penetrates into the pore entrances, forming curved interfaces due to the solid-liquid contact angle θ. The total area of the vapor-liquid interfaces is then equal to ϕ_s times the membrane area, times a curvature correction factor assuming that the surface takes the shape of a spherical partition [26]

$$f_{\mathrm{W}} = \frac{2}{1+\sin(\theta)}, \tag{23}$$

while the total area of the fluid-solid contact is $1-\phi_s$ times the total area. In the Cassie-Baxter state, the liquid rests on protruding asperities on the surface, and the fluid-solid contact area fraction can be estimated as [26]

$$\alpha_{\mathrm{CB}} = \frac{1+\cos(\theta)}{1+\cos(\theta_e)}, \tag{24}$$

where θ_e is the "intrinsic" contact angle between the liquid and a smooth surface of the same material. If we approximate the vapor-liquid interface in the CB state to be planar, the area of exposed vapor-liquid interface is $1-\alpha_{\mathrm{CB}}$. We see that it is possible to obtain large effective evaporation areas in both states – in the W state due to strong surface curvature, and in the CB state due to a smaller proportion of direct liquid-solid contact. Neglecting surface curvature effects on the resistivities of the vapor-liquid interface [27], the W state interface resistivities are

$$\begin{aligned} R_{uu}^{\mathrm{W}} &= \left(\frac{\phi_s f_{\mathrm{W}}}{R_{uu}^{\mathrm{gl}}} + \frac{1-\phi_s}{R_{qq}^{ls}}\right)^{-1}, \\ R_{um}^{\mathrm{W}} &= -R_{uu}^{\mathrm{W}} Q_{\mathrm{gl}}^*, \\ R_{mm}^{\mathrm{W}} &= \frac{R_{mm}^{\mathrm{gl}}}{\phi_s f_{\mathrm{W}}} + \frac{R_{uu}^{\mathrm{W}} - R_{uu}^{\mathrm{gl}}}{\phi_s f_{\mathrm{W}}} Q_{\mathrm{gl}}^{*\,2}, \end{aligned} \tag{25}$$

where $Q_{\mathrm{gl}}^* = -r_{um}^{\mathrm{gl}}/r_{uu}^{\mathrm{gl}}$ is the energy of transfer across the vapor-liquid interface, and R_{qq}^{ls} is the thermal resistance of the liquid-solid contact. The liquid-solid contact typically makes the thermal resistance of the interface smaller than that of the vapor-liquid interface by itself. The CB state gives slightly different conductivities. Neglecting any additional resistance due to diffusion processes tangentially to the membrane surface, we obtain

$$\begin{aligned} R_{uu}^{\mathrm{CB}} &= \left(\frac{1-\alpha_{\mathrm{CB}}}{R_{uu}^{\mathrm{gl}}} + \frac{\alpha_{\mathrm{CB}}}{R_{qq}^{ls}}\right)^{-1}, \\ R_{um}^{\mathrm{CB}} &= -R_{uu}^{\mathrm{CB}} Q_{\mathrm{gl}}^*, \\ R_{mm}^{\mathrm{CB}} &= \frac{R_{mm}^{\mathrm{gl}}}{1-\alpha_{\mathrm{CB}}} + \frac{R_{uu}^{\mathrm{CB}} - R_{uu}^{\mathrm{gl}}}{1-\alpha_{\mathrm{CB}}} Q_{\mathrm{gl}}^{*\,2}. \end{aligned} \tag{26}$$

Depending on the wetting state of the surface, either Eq. (25) or Eq. (26) are inserted into Eq. (7) to determine $R_{ij}^{s,1}$ and $R_{ij}^{s,2}$. In summary, we have

$$R_{ij}^{s,k} = \begin{cases} R_{ij}^{\mathrm{W}} & \text{surface } k \text{ in Wenzel state.} \\ R_{ij}^{\mathrm{CB}} & \text{surface } k \text{ in Cassie} - \text{Baxter state.} \end{cases} \tag{27}$$

3.3. Temperature polarization

Separating the bulk liquid and the membrane-liquid interface is a stagnant diffusion layer where the thermal resistance of the bulk liquid must be taken into account. We characterize this region as a layer of stagnant liquid with an effective thickness δ^{pol}, and neglect any composition gradients in this layer. The thermal resistance of this layer is then

$$R_{qq}^{p} = \delta^{\mathrm{pol}} r_{qq}^{w}, \tag{28}$$

where r_{qq}^{w} is the thermal resistivity of water. This is more commonly expressed in terms of the dimensionless Nusselt number Nu. This relates to our effective layer thickness as follows:

$$\delta^{\mathrm{pol}} = \frac{L_h}{\mathrm{Nu}} \tag{29}$$

where L_h is the characteristic length scale involved in the calculation of Nu itself, typically the hydraulic diameter of the flow channel. In general, the Nusselt number in a typical flow channel parallel to a mem-

brane surface is correlated to the Reynolds number Re and the Prandtl number Pr in the following way [28]

$$\mathrm{Nu} \propto f \mathrm{Re}\mathrm{Pr}^{1/3}, \tag{30}$$

where f is the friction factor, which depends on the hydraulic diameter and the membrane surface roughness. When f is known for the particular flow channel and membrane, the temperature dependence of the layer thickness can be obtained via the dependence of f, Re and Pr on the kinematic viscosity and the thermal diffusivity of the liquid.

The practical consequence of temperature polarization is that the temperatures of the two vapor-liquid interfaces differ from the temperatures of the adjacent bulk liquids

$$T_1^{s,l} = T_1 - \frac{\delta_1^{\mathrm{pol}} J_u}{\lambda_1^w}, \quad T_2^{s,l} = T_2 + \frac{\delta_2^{\mathrm{pol}} J_u}{\lambda_2^w}, \tag{31}$$

where $T_1^{s,l}$ and $T_2^{s,l}$ are the liquid temperatures close to the vapor-liquid interfaces, as indicated in Fig. 1; λ_1^w and λ_2^w is the thermal conductivity of water evaluated on the two sides at the average temperature of each respective polarization layer. In practice, this is typically seen as reducing the effective temperature difference by a factor Θ, known as the temperature polarization coefficient (TPC). We define it here by the relation

$$T_2^{s,l} - T_1^{s,l} = \left[1 + \frac{J_u}{\Delta_{1,2}T}\left(\frac{\delta_1^{\mathrm{pol}}}{\lambda_1^w} + \frac{\delta_2^{\mathrm{pol}}}{\lambda_2^w}\right)\right]\Delta_{1,2}T = \Theta\Delta_{1,2}T. \tag{32}$$

The effective thickness δ^{pol} depends on the liquid flow conditions near the membrane, and is the parameter that explains the correlation between Θ and the Nusselt number, thoroughly assessed by Khayet et al. in [29]. Promoting turbulent flow gives a smaller δ^{pol}, bringing Θ closer to unity. Since the Nusselt number depends on the local viscosity and thermal diffusivity, this treatment of temperature polarization will in general give different thermal resistances in the two polarization layers due primarily to the temperature dependence of the local viscosity and thermal diffusivity, thus affecting the temperatures of the two liquid-membrane surfaces differently. Due to the exponential dependence of the equilibrium vapor pressure on the interfacial temperature, this phenomenon can have a significant impact on the distillation process.

3.4. Overall transport coefficients

Most of the MD processes described in the literature are limited by the resistances of the membrane bulk. That is, the resistances of the membrane bulk are much larger than those of the liquid-membrane interfaces, such that the transport properties of the system are to a good approximation given entirely by the transport properties of the membrane bulk plus the effects of temperature polarization [3]. For this reason, we choose to present the contributions from the liquid-membrane interfaces here in the form of correction factors to the membrane bulk coefficients. We develop in Appendix A a correction factor formalism that expresses the transport coefficients of the membrane system as those of the bulk membrane times correction factors that take the resistances of the interface regions Γ_i^s into account. In terms of the factors derived in Appendix A, we present the apparent diffusion coefficient

$$D_{\mathrm{m}}^{\mathrm{eff}} = D_m\left(\mathscr{B}_{mm} + Q_m^*\mathscr{B}_{um}\right) \tag{33}$$

and the energy of transfer

$$Q_m^{*,\mathrm{eff}} = Q_m^* + \frac{R^2\overline{T}^3\lambda_m}{\widehat{p}_w^* D_m}\left(Q_m^* + \frac{\mathscr{B}_{um}}{\mathscr{B}_{mm}}\right)^{-1} \tag{34}$$

and the thermal conductance

$$\Lambda_{\mathrm{m}}^{\mathrm{eff}} = \frac{\lambda_m}{\delta}\mathscr{B}_{uu} + \frac{\widehat{p}_w D_m^{\mathrm{eff}}}{R^2\overline{T}^3\delta}\left[\frac{Q_m^{*\,2}\mathscr{B}_{uu} + Q_m^*\mathscr{B}_{mu}}{\mathscr{B}_{mm} + Q_m^*\mathscr{B}_{um}} - Q_{\mathrm{tot}}^{*\,2}\right] \tag{35}$$

where the $\mathscr{B}_{ij}$ are defined in Appendix A, and we point out, importantly, that $\mathscr{B}_{mu} \neq \mathscr{B}_{um}$. The permeability L_p is related to D_m^{eff} as

$$L_p = \frac{V_w\widehat{p}_w D_m^{\mathrm{eff}}}{R^2\overline{T}^2\delta}. \tag{36}$$

We rewrite the heat of transfer as

$$q_{\mathrm{tot}}^* = Q_{\mathrm{tot}}^* - H_{w,l} = Q_{\mathrm{tot}}^* - H_{w,g} + \Delta_{\mathrm{vap}}H_w = q_m^* + \Delta_{\mathrm{vap}}H_w, \tag{37}$$

where subscripts l and g refer to the liquid and gas phases. We have written the total heat of transfer as a sum of two terms, where one of them is the enthalpy of vaporization, $\Delta_{\mathrm{vap}}H_w$. The other term, $q_m^* = Q_{\mathrm{tot}}^* - H_{w,g}$, is a combination of the heat of transfer on the vapor side of the interfaces and in the membrane bulk. The thermo-osmotic coefficient can then be expressed as

$$D_{\mathrm{T}}^{\mathrm{eff}} = \frac{\widehat{p}_w D_m^{\mathrm{eff}}}{R^2\overline{T}^3\delta}\left(q_m^* + \Delta_{\mathrm{vap}}H_w\right), \tag{38}$$

which is the most important quantity for MD applications. We remark that the observed thermal conductance Λ_{tot} and the observed thermo-osmotic coefficient D_T as defined in Eq. (4) are obtained considering the total temperature difference $\Delta_{1,2}T$ across the system, while the quantities defined in this section pertain only to the membrane system excluding the polarization layers, with the driving force $T_2^{s,l} - T_1^{s,l} = \Theta\Delta_{1,2}T$. The observed quantities are therefore adjusted by the TPC as follows

$$D_T = \Theta D_T^{\mathrm{eff}}, \quad \Lambda_{\mathrm{tot}} = \Theta\Lambda_m^{\mathrm{eff}}. \tag{39}$$

3.5. Summary of theory

We can now use the following procedure for constructing the transport coefficients of the membrane system: When the thermal conductivity, heat of transfer, and diffusivity in the limits $\mathrm{Kn}\to 0$ and $\mathrm{Kn}\to\infty$ are known, the coefficients for a single pore can be calculated by Eq. (12). Given the pore size distribution, porosity, tortuosity, and solid thermal conductivity, the bulk membrane parameters are obtained by Eqs. (17), (18), and (19), where the statistical correction factors are defined in Eq. (15). These parameters are then corrected for interfacial contributions by calculating the correction terms summarized in Appendix A and inserting them into Eqs. (35), (34), and (33). The final link to the observable coefficients in Eq. (4) is then provided by Eqs. (36) and (38), with adjustments for temperature polarization given by Eq. (39).

The outlined procedure gives the first approximations to the observed transport coefficients of the membrane system. In order to account for nonlinear effects that occur at more extreme conditions, the local values of the bulk transport coefficients must be calculated by the iterative method outlined in Appendix B in order to provide more accurate values for the total resistances of the membrane bulk.

4. Results and discussion

In Section 3, we provided a systematic method for describing the transport coefficients defined in Eq. (4) from knowledge of the pore size distribution, porosity, tortuosity, contact angle, and knowledge of the transport properties of the vapor-liquid interface and the wetting state of the surface. In order to facilitate correspondence with most of the MD literature, we provided in Section 3.4 the transport coefficients of the system in the form of membrane bulk properties times correction factors defined in Appendix A to account for interfacial contributions. In the following, we will refer to the full model represented by Eq. (38) as the

non-equilibrium thermodynamics (NET) approach. The more commonly used Eq. (43) will be referred to as the simplified model.

In Section 4.1, we will demonstrate that the simplified model is a special case of the NET approach with appropriate approximations. We proceed to use this correspondence to compare the methods for the Millipore DuraPore GVHP membrane in Section 4.2. Here, we justify the simplified model on quantitative grounds, and propose a simple correction factor that corrects for most of the discrepancies with respect to the NET approach. We discuss two cases in Sections 4.3 and 4.4 where the predictions from the NET approach diverge from the simplified model.

4.1. Correspondence to membrane distillation literature

We will next discuss the link that explains the difference between Eq. (38) and the ubiquitous notion that the primary driving force of the process of MD is the difference in the vapor saturation pressure across the system due to the difference in temperature. It is well established that two features are routinely neglected: the interfacial contributions to the total resistances, and the kinetic heat-mass coupling. The latter gives rise to the assumption that $|q_m^*| \ll \Delta_{\text{vap}} H_w$. If we also neglect interfacial effects and effects of the pore size distribution, then $D_m^{\text{eff}} \approx \phi_s D_c(\bar{a})/\tau_p$. The thermo-osmotic coefficient is then

$$D_{\text{T}}^{\text{eff}} \approx \frac{\phi_s \widehat{p}_w D_c(\bar{a})}{R^2 \bar{T}^3 \tau_p \delta} \Delta_{\text{vap}} H_w. \tag{40}$$

From the Gibbs-Duhem relation for liquid water in equilibrium with its vapor, one obtains the Clausius-Clapeyron equation

$$\left(\frac{\partial p_w^{\text{sat}}}{\partial T}\right)_m = \frac{p_w^{\text{sat}} \Delta_{\text{vap}} H_w}{RT^2}. \tag{41}$$

Assuming that the vapor is saturated, such that $\widehat{p}_w = p_w^{\text{sat}}(\bar{T})$, then

$$D_{\text{T}}^{\text{eff}} \approx \frac{\phi_s D_c(\bar{a})}{R\bar{T}\tau_p \delta} \left(\frac{\partial p_w^{\text{sat}}}{\partial T}\right)_m \Bigg|_{T=\bar{T}}. \tag{42}$$

The water flux is proportional to D_T times the difference in temperature between the two liquid-vapor interfaces. We may again approximate

$$J_w \propto -D_T^{\text{eff}} \left(T_2^{s,l} - T_1^{s,l}\right) \approx -\frac{\phi_s D_c(\bar{a})}{R\bar{T}\tau_p \delta} \Delta p_w^{\text{sat}}. \tag{43}$$

This expression, which can be read as the gas permeance of the membrane times the difference in the water saturation pressure is commonly encountered in the MD literature [3], where the saturation pressure difference is usually quoted as the main driving force. The true thermal driving force is the temperature difference, which is more general because it does not depend on the properties of the vapor-liquid equilibrium, and includes heat-mass coupling effects that had to be neglected in order to arrive at Eq. (43). When interfacial contributions are negligible and the pore radius is much larger than the interaction range between the molecules and the pore walls, specified in Ref. [21], q_m^* is negative with a maximum absolute value $RT/2$, which accounts for roughly 6–7% of the sum $q_m^* + \Delta_{\text{vap}} H_w$. This means that neglecting q_m^* is reasonable as long as the statistical uncertainty in the measurements is greater than 6–7%. Interpretation of more accurate experiments, especially with smaller pores, should include q_m^* by using the full expression in Eq. (38).

4.2. Case study: the DuraPore GVHP membrane

We will next compare results from the NET approach and the simplified model for the well-studied case of the Millipore DuraPore GVHP membrane.

Khayet et al. assumed a log-normal pore size distribution and obtained a mean pore radius of 133 nm and geometric standard deviation of 1.12 by means of the wet/dry flow method [30]. In the same study, they also obtained a mean pore tortuosity equal to 2.14, and the thickness of the membrane was 117.7 μm. The porosity of the membrane was found to be 70.1% and its bulk thermal conductivity 41 mW/m [31]. García-Payo et al. also determined the advancing contact angle to be 111° [32]. We determine that this angle is too small for the surface to be in the Cassie-Baxter mode, as this would give a solid-liquid contact area greater than $1 - \phi_s$, which is nonphysical with the present assumptions. We therefore assume that the wetting state of the surface is of the Wenzel kind.

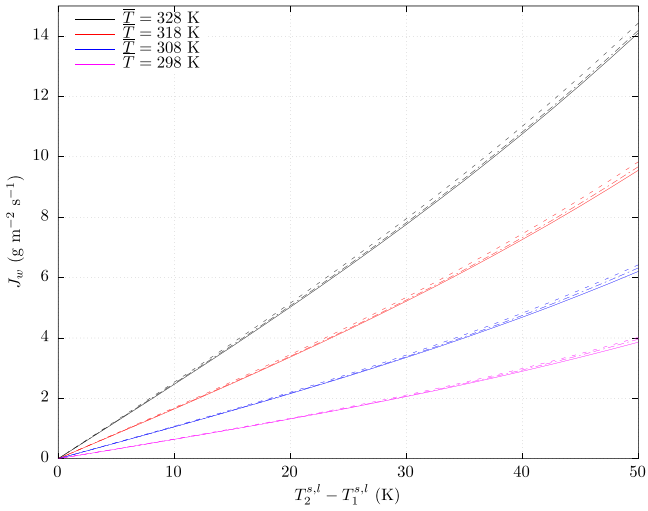

Fig. 2. Predicted water flux through a GVHP membrane in a DCMD configuration, with pure water on both sides, as a function of the temperature difference $T_2^{s,l} - T_1^{s,l}$ across the system at different mean temperatures $\bar{T}$. The solid lines are predictions by the NET approach; the dashed lines represent the simplified model prevalent in MD literature (Eq. (43)). The dash-dotted lines represent the model with a corrected heat of transfer according to Eq. (45).

In Fig. 2, we show the predicted water fluxes with distilled water on both sides of the GVHP membrane using the parameters listed in the preceding paragraph, as functions of the temperature difference at different mean temperatures. The NET approach is represented by solid lines, and the values predicted by the simplified model are represented by the dashed lines. The simplified model systematically overpredicts the flux compared to the full model, in the range considered here by up to 3%. We will next investigate the correction terms systematically.

Numerical evaluation of the total energy of transfer in Eq. (34) indicates that the second term accounts for a relative correction on the order 10^{-7}, such that for all practical purposes $Q_{\text{tot}}^* = Q_m^*$. Furthermore, a deviation of $\mathscr{K}_{\sigma,um}/\mathscr{K}_{\sigma,mm}$ from unity is on the order of 10^{-5}, so by Eq. (18) it is reasonable to take $Q_m^* = Q_p^*(\bar{a})$. In summary, the total energy of transfer of the membrane system is for all practical purposes equal to the energy of transfer in the average pore. Thus,

$$q_m^* = \frac{\lambda_{\text{K}}(\bar{a}) q_h^* + \lambda_h q_{\text{K}}^*(\bar{a})}{\lambda_{\text{K}}(\bar{a}) + \lambda_h} \tag{44}$$

which is negative with an absolute value up to 3% of the total $q_m^* + \Delta_{\text{vap}} H_w$ in the GVHP membrane, so that neglecting q_m^* accounts for most of the overprediction by the simplified equation. Since q_m^* is larger in absolute value in smaller pores, the error made by using the simplified model will be greater in smaller pores. In pores where the radius is comparable to the range of the intermolecular interaction between individual water molecules and the pore walls, q_m^* can take much larger values and also change sign. For a detailed exposition, see [21]. Based on this analysis, a straightforward improvement of Eq. (43) can be obtained

by using the correction factor $1 + q_m^*/\Delta_{\text{vap}}H_w$ as follows

$$J_w \approx -\frac{\phi_s D_c(\bar{a})}{R\bar{T}\tau_p\delta}\left(1+\frac{q_m^*}{\Delta_{\text{vap}}H_w}\right)\Delta p_w^{\text{sat}}, \tag{45}$$

which captures some of the discrepancy between the NET approach and the simplified model, especially for membranes with small pores.

The interfacial resistances are in this case given by those of the Wenzel mode (Eq. (25)). Given our assumption that molecules that pass through the liquid-vapor interface thermalize shortly with the pore walls, the thermal conductance of the interface is dominated by the greatest of that of the liquid-vapor interface and that of the liquid-solid contact.

Calculations then indicate that in the present case, the interfacial thermal resistance is 5 orders of magnitude smaller than that of the membrane bulk, which justifies neglecting any temperature jumps at the interfaces. This also means that the effect of the interface must be due to its contribution to the mass transfer resistance of the system, which is contained in the correction factor $\mathscr{B}_{mm} + Q_m^*\mathscr{B}_{um}$ to the apparent diffusion coefficient. Furthermore, since the correction due to the effect of the pore size distribution is also a common factor to the apparent diffusion coefficient, it is convenient to see these two corrections in combination. Both the interfacial term and the correction factor $\mathscr{K}_{\sigma,mm}$ are plotted in Fig. 3 as functions of the mean temperature of the GVHP system, along with the product of the two corrections to give the net effect of both contributions. As it must, the correction factor $\mathscr{B}_{mm} + Q_m^*\mathscr{B}_{um}$ is smaller than unity, because the interfaces can only increase the mass transfer resistance of the system. On the other hand, variation in pore size tends to decrease the mass transfer resistance of the membrane, thus increasing the apparent diffusion coefficient by a factor greater than unity. Both corrections account for less than 1%, and their combination even less. This justifies neglecting both effects, as they in combination account for at most a 0.5% net correction.

The remainder of the deviation between the NET approach and the simplified model comes from nonlinear effects that originate in the dependence of the local resistivities on the local thermodynamic variables. We call these effects nonlinear in the sense that they give the appearance that the flux deviates from a straight line as a function of the temperature difference. The most important among these effects is in a subtle way already captured by Eq. (43) in the step where the temperature derivative of the saturation pressure times the temperature difference is taken to be equal to the difference in the saturation pressure. Since the saturation pressure depends exponentially on the local temperature, Eq. (43) is already beyond the linear approximation $J_w \propto T_2^{s,l} - T_1^{s,l}$, which is precisely the motivation behind the recommendation by Khayet and Matsuura to use $p_w^{\text{sat}}\left(T_2^{s,l}\right) - p_w^{\text{sat}}\left(T_1^{s,l}\right)$ instead of $T_2^{s,l} - T_1^{s,l}$ as the effective driving force when the temperature difference is large [3].

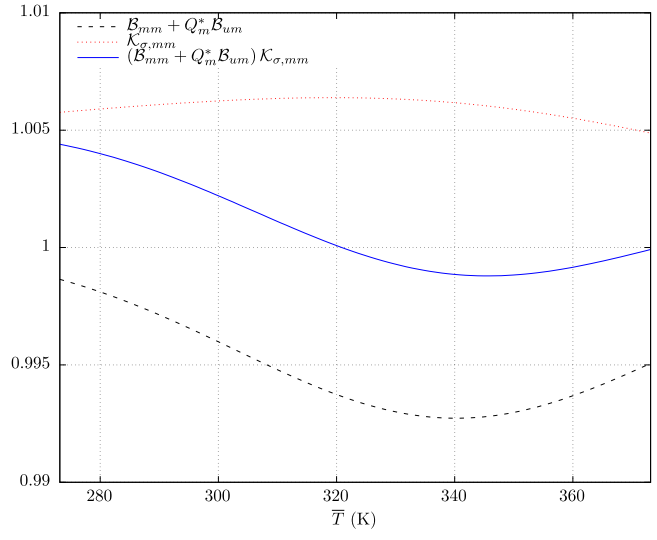

Fig. 3. Correction factor to the apparent diffusion coefficient due to the pore size distribution, $\mathscr{K}_{\sigma,mm}$, correction factor due to interfacial resistances, $\mathscr{B}_{mm} + Q_m^*\mathscr{B}_{um}$, and their product, as function of the mean temperature of the Dura-Pore GVHP membrane system.

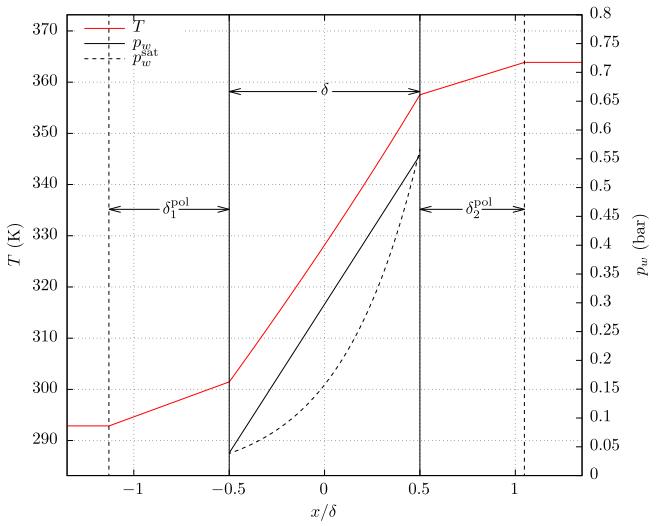

Fig. 4. Profiles predicted by the NET approach of temperature T, water vapor pressure p_w, and pure water saturation pressure p_w^{sat} through a GVHP membrane in DCMD configuration with liquid temperatures 292.9 K and 363.9 K, with distilled water on the cold side and 1 mol/kg aqueous NaCl solution on the hot side. The polarization layer thicknesses are roughly 74 m on the cold side and 64 m on the hot side.

The apparent nonlinearity that occurs at large temperature differences can be understood by observing the temperature dependence of the bulk transport coefficients. In Fig. 4, we have plotted the calculated profiles for the temperature, water partial pressure, and local saturation pressure across the GVHP membrane in an extreme case with a temperature difference of 71 K and a 1 mol/kg NaCl solution on the feed side. The temperature profile deviates only slightly from a straight line due to the dependence of the local thermal conductivity on the local temperature, and also due to the heat carried locally by the steady state mass flux through the pores, which is exchanged with the pore walls as the molecules thermalize. The mass transfer resistance of the membrane varies significantly through the membrane because of its dependence on the local temperature and water vapor concentration. The resulting bottlenecks are not taken into account by merely evaluating the transport coefficients at the mean temperature and geometric mean concentration, leading to a significant difference between the first approximation and the transport coefficients obtained by numerical integration from the local level.

We can also observe in Fig. 4 that the local saturation pressure, represented by the dashed line, is very different from the local partial pressure through the membrane. The mass transfer conductivity is proportional to the local concentration of water molecules, and an initial guess to the steady state profile is that the product of this conductivity and the chemical potential gradient, proportional to the gradient in the logarithm of the concentration, is constant. This means that we should expect that the steady state concentration gradient is roughly constant, giving a linear partial pressure profile. The saturation pressure, on the other hand, depends exponentially on the local temperature. The result is that the vapor inside the membrane pores is supersaturated to varying degrees with respect to equilibrium with a flat surface of liquid water. This is probably stabilized by the confinement of the gas mixture inside

the porous structures, which provides an energy barrier for the transition to liquid phase [33,34]. While this increase in water concentration tends to increase the mass transfer conductivity of the pore with respect to water vapor, it also contributes to an increase in the overall pressure of the gas mixture, leading to increased mass transfer resistance in larger pores due to an increased rate of intermolecular scattering.

We conclude the case study by comparing predicted values to water fluxes reported in the literature. In general, both the NET-approach and the simplified model overpredict the net mass flux of water compared to experiments. The reason for this is temperature polarization, explained in Section 3.3. Extensive work on this phenomenon was carried out by Khayet et al. [11], where the temperature polarization coefficient (TPC), Θ, was correlated to the flow conditions in the bulk liquids. They reported a TPC for the GVHP system between 0.6 and 0.5 at laminar flow conditions, and between 0.96 and 0.93 for turbulent flow conditions. For example, their GVHP case with liquid temperatures 292.9 K and 363.9 K resulted in a flux 13.52 $\mathrm{g\,m^{-2}\,s^{-1}}$, whereas the NET approach and the simplified model with no temperature polarization predict 21.53 and 22.39 $\mathrm{g\,m^{-2}\,s^{-1}}$, respectively. Adjusting the simplified model by factoring in the correction of Eq. (45) gives a better agreement with the NET approach at 22.00 $\mathrm{g\,m^{-2}\,s^{-1}}$. To incorporate temperature polarization, we will apply the NET approach.

We use the polarization layer thickness δ_1^{pol} as an adjustment parameter, and use the correlation in Eq. (30) to determine δ_2^{pol}. For laminar flow, $f \propto \mathrm{Re}^{-1/2}$ [28], and we obtain from standard expressions for Re and Pr, assuming that the flow channel geometry and flow rates are the same on both sides

$$\frac{\delta_2^{\mathrm{pol}}}{\delta_1^{\mathrm{pol}}} = \left(\frac{\alpha_{w,2}\sqrt{\nu_{w,2}}}{\alpha_{w,1}\sqrt{\nu_{w,1}}} \right)^{1/3}, \tag{46}$$

where $\alpha_{w,i}$ is the average thermal diffusivity and $\nu_{w,i}$ the average kinematic viscosity of the liquid in the polarization layers. In this particular case, we obtain the experimentally reported flux when $\delta_1^{\mathrm{pol}} \approx 74$ μm and $\delta_2^{\mathrm{pol}} \approx 64$ μm, which is illustrated to scale in Fig. 4. The resulting TPC is roughly 0.79.

This case study demonstrates that the approximations leading to Eq. (43) are adequate for the GVHP system, and the two approaches give roughly the same results after the recommended refinements to the simplified model. This explains why Eq. (43) is so successful – the effects that are neglected are not important in the systems that have historically been considered in the MD literature. Neglecting q_m^* gives a consistent 2–3% overprediction, which is typically not sufficient to be distinguishable from experimental noise. We will next, however, make predictions where the two approaches give very different result and the NET approach provides additional insight.

4.3. Case: liquid-vapor interface separated from membrane

Consider the Cassie-Baxter wetting state, and let the contact angle $\theta \to \pi$. In this limit, the liquid-solid contact vanishes, and we have a liquid-vapor interface that is completely separated from the membrane surface. This situation was investigated for a single component system with molecular simulations by Rauter et al. [16], and can also be considered to be a special case of the vapor-gap MD configuration in the limit as the thickness of the air gap goes to zero, and the interfacial resistances are those of a plane liquid-vapor interface. This is an interesting case because the magnitude of the interfacial thermal resistance is comparable to that of the membrane. We will henceforth refer to this case as the CB state.

As can be seen in Fig. 5, when the thermal resistance of the interface is dominated by that of the vapor-liquid interface, we obtain significant

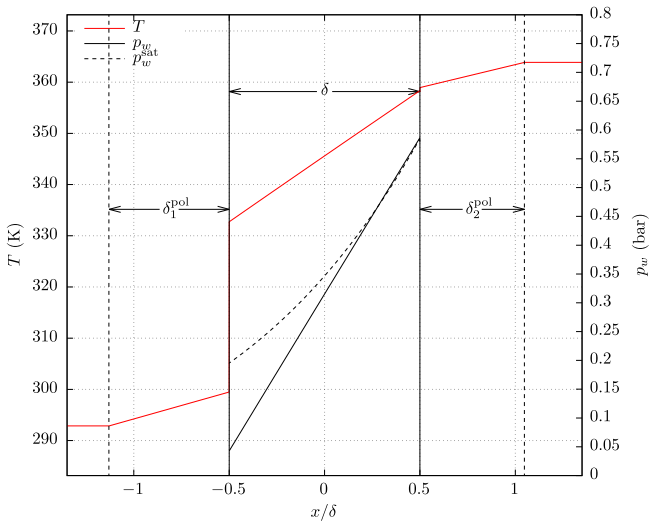

Fig. 5. Predicted profiles of temperature T, water vapor pressure p_w, and pure water saturation pressure p_w^{sat} through a model GVHP membrane in DCMD configuration with liquid temperatures 292.9 K and 363.9 K, with distilled water on the cold side and 1 mol/kg aqueous NaCl solution on the hot side, with the vapor-liquid interfaces separated from the membrane by a negligible distance (CB state). The polarization layer thicknesses are roughly 74 μm on the cold side and 64 μm on the hot side.

temperature jumps. The thermal resistance of the interface depends exponentially on the temperature of the interface, which is typically found to be roughly equal to that of the liquid phase close to the interface [24]. The temperature jump is therefore more pronounced on the cold side, because the interfacial resistance is larger there than on the hot side. This leads to the tendency that the vapor is unsaturated on the cold side and supersaturated on the hot side. The average temperature in the membrane is higher than in the Wenzel case shown in Fig. 4. The mass transfer resistance of the membrane tends to decrease with temperature due to increased particle momentum, but also tends to increase due to the higher particle concentration leading to more frequent scattering. Due to these competing effects, the pore diffusion coefficient attains a maximum value at roughly 328 K for membranes that were initially in equilibrium with humid air at room temperature.

In the CB state version of our GVHP case study, the water flux is predicted to be 13.86 $\mathrm{g\,m^{-2}\,s^{-1}}$, which is a 3% increase compared to the W case. The primary reason for the flux enhancement is that the higher thermal resistance across the interfaces leads to an increase in the overall thermal resistance of the system, thus lowering the energy flux through the system. The thermal resistance of the polarization layers being roughly the same in both cases, this leads to a reduction in the temperature drop across these layers. The TPC has in this case increased from 0.79 to 0.84. We show in Fig. 6 how the predicted CB state flux and TPC compare to the W state flux and TPC as functions of the temperature difference at different mean temperatures. The TPC is clearly larger in the CB state in all cases, and there is a clear tendency for the TPC to decrease with temperature, due to the increase in the membrane thermal resistance. The difference in TPC between the W and CB states is greater at lower temperatures, where the thermal resistance of the liquid-vapor interface is higher. When the temperature difference is very small, we see that the water flux changes sign due to the osmotic flux that is driven by the difference in salt concentration. The accompanying heat of transfer gives a substantial heat flux from distillate to feed, leading to cases where a TPC greater than unity is possible.

An interesting finding by Rauter et al. is that the CB state tends to enhance the mass flux up to a certain point dictated by the mass transfer

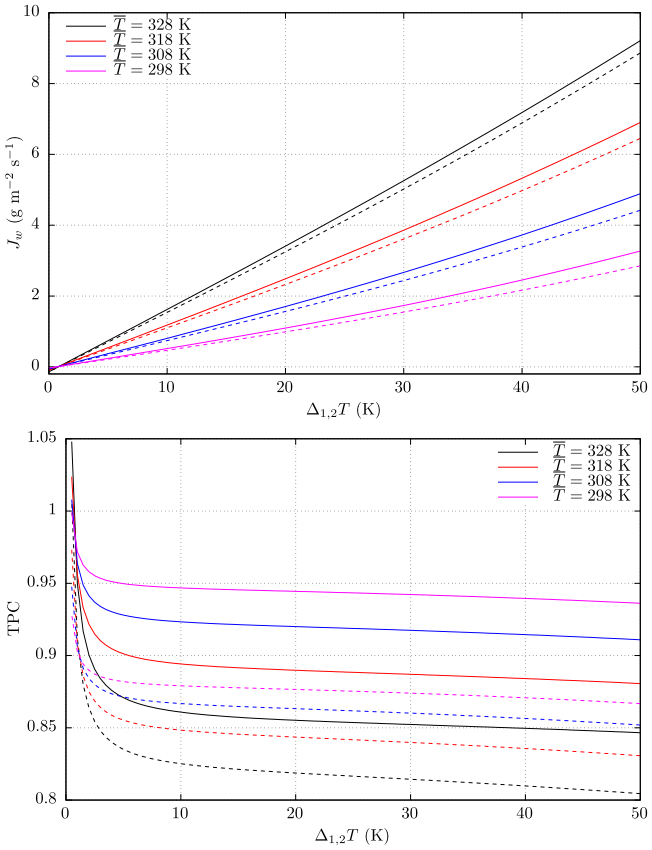

Fig. 6. Top: Predicted water flux through a GVHP membrane in a DCMD configuration, with pure water on the distillate side and a 1 mol/kg NaCl feed solution, as a function of the temperature difference $\Delta_{1,2}T$ across the system at different mean temperatures $\bar{T}$. The polarization layer thickness is 74 μm at 292.9 K, and its variation with temperature is given by Eq. (46). Solid lines indicate predicted values in the case that the vapor-liquid interfaces are separated from the membrane (CB state), while the dashed lines indicate the reference Wenzel state with contact angle 111°C. Bottom: The temperature polarization coefficient (TPC) corresponding to the cases in the top figure.

resistance of the porous medium [16]. Since the mass transfer resistance in the GVHP system is dominated by that of the bulk membrane, the decrease in interfacial mass transfer resistance that accompanies a transition to the CB state has negligible effect on the flux in this particular system.

4.4. Case: nanometer scale pores

When the pore-sizes approach the nanometer scale, we can no longer neglect the effect of direct interactions between the molecules and the pore walls. Although we do not have the parameter values ε and σ, corresponding to the interaction energy and range in the model detailed in [21], we can estimate some values based on the investigation by Rauter et al. [16]. In the latter work, the wetting parameter α was adjusted to reproduce liquid-solid contact angles. For the fluid-wall interaction, they used the Lennard-Jones/spline model with interaction energy $\varepsilon_w/k_B = 741$ K and a molecular diameter $\sigma_w = 3.25$ Å. With a wetting parameter $\alpha = 0.5$, which is expected to give a slightly larger contact angle than the 103° that was obtained with $\alpha = 0.6$, matching the total barrier energy and minimizing the difference between the first approximations to the radial distribution functions $\exp(-\beta\varphi(r))$ gives the values $\varepsilon = 2\varepsilon_w/5$ and $\sigma = 0.52\sigma_w$. These values allow us to calculate the corrections to the Knudsen limit for this hypothetical system.

Based on these parameter values, we show in Fig. 7 the predicted dependence of D_c and q_m^* on the pore radius a at temperature 298 K. The

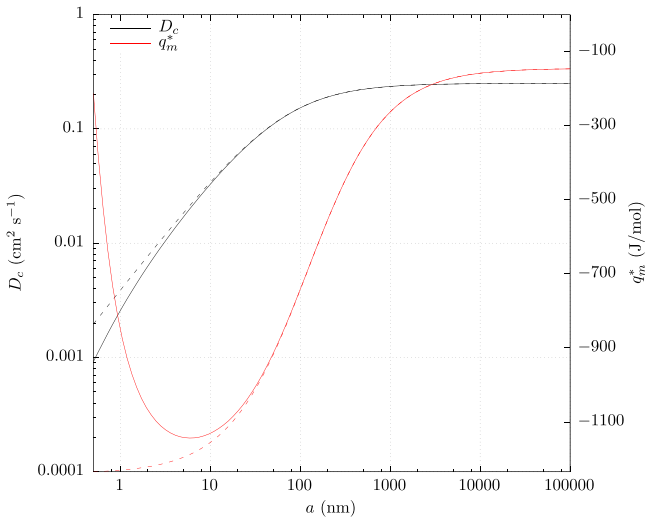

Fig. 7. The pore diffusion coefficient D_c and membrane gas heat of transfer q_m^* as function of the pore radius a, corrected for the hydrophobic fluid-wall interaction (solid lines), compared to predictions not corrected for the interaction (dashed lines), at temperature 298 K.

dashed lines indicate the values that are not corrected for the fluid-wall interaction. The heat of transfer contribution q_m^* dips towards the Knudsen value of $-RT/2$ before increasing in nanometer scale pores due to sorption effects. The Knudsen model (dashed curve) overpredicts the pore diffusion coefficient in small pores. The net effect is that D_T is expected to be significantly smaller in nanometer pores than would be predicted without the sorption corrections. In applications where nanometer scale pores are important, such as in systems where the membrane must maintain a large pressure difference, it may be important to take such corrections into consideration.

5. Conclusions

Membrane distillation (MD) is used as an umbrella term for processes that utilize membranes as transport media to facilitate distillation of volatile components at operating temperatures generally below the boiling point of either component at the given conditions. To enhance the understanding of transport mechanisms at play in MD systems, we have presented a systematic non-equilibrium thermodynamics (NET) procedure to describe the observed macroscopic transport properties of the membrane system from knowledge of the structural and chemical properties of the membrane. The method integrates the transport properties of the membrane, the interfaces, and temperature polarization in a manner justified by fundamental conservation laws. This provides a coherent and unified approach to assess all the transport phenomena in combination, including mass transfer, heat transfer, and coupling effects between the two. The NET approach reveals that the temperature difference across the membrane is the true driving force of mass transfer, which after suitable approximations is equivalent to the saturation pressure difference.

To demonstrate the approach and its applicability, we discuss case studies that showcase both correspondence to models used in MD literature, and cases where commonly used models fall short. Through a series of approximations, e.g. that the resistance to transport is dominated by the bulk membrane, we arrived at Eq. (43), which is a commonly used formula for the distillate flux. It was demonstrated that this formula systematically overpredicts the flux compared to results from the NET approach, primarily due to neglecting the kinetic heat-mass coupling effects and due to the dependence of the local mass transfer resistance on the local thermodynamic state. The former is more

important in small pores, and can account for up to 6% overprediction in the Knudsen limit. In the GVHP membrane in particular, correcting the simplified model for the kinetic heat of transfer brought the overprediction of 3% down to 0.5%. To obtain a better agreement with the NET approach, we recommend using the correction factor in Eq. (45) to account for the commonly neglected kinetic heat-mass coupling.

To better understand the role of interfacial transport phenomena, we have investigated the hypothetical case where the liquid-vapor interface is completely separated from the membrane surface as a representation of a Cassie-Baxter wetting state. The thermal resistance of the vapor-liquid interface is then comparable to that of the bulk membrane, so that the thermal resistance of the system is significantly increased. This leads to a enhancement of the mass flux by up to 3% due to the lowered energy flux, which reduces the effect of temperature polarization and provides a larger temperature difference between the two liquid-vapor interfaces.

The development of the formula in Eq. (11) for the addition of transport resistivities at the pore level gives a straightforward way to implement the transport coefficients for hydrophobic nanoscale pores. This is especially relevant for pressure-retarded MD processes where small pores are required to prevent liquid penetration at elevated pressures. Predictions from the NET approach indicate that the mass transfer resistance of nanoscale pores can be much smaller than that predicted by the Knudsen model, which is an important factor to consider when designing pressure-retarded systems. The systematic NET approach allows the construction of a complete model for transport phenomena through a membrane system where nanoscale effects can also be taken into account.

In conclusion, the systematic NET approach presented in this work offers a coherent and unified framework for understanding and assessing the transport phenomena in MD processes, which can be used to tailor their properties for enhanced performance.

CRediT authorship contribution statement

Kim R. Kristiansen: Conceptualization, Methodology, Formal analysis, Software, Validation, Visualization, Writing – original draft, Writing – review & editing. **Øivind Wilhelmsen:** Conceptualization, Supervision, Writing – original draft, Writing – review & editing. **Signe Kjelstrup:** Conceptualization, Supervision, Project administration, Writing – original draft, Writing – review & editing.

Declaration of competing interest

The authors declare the following financial interests/personal relationships which may be considered as potential competing interests: Kim Kristiansen reports financial support was provided by Research Council of Norway.

Data availability

Data will be made available on request.

Acknowledgements

The authors are grateful to the Research Council of Norway through its Centers of Excellence funding scheme, Project No. 262644, PoreLab, and to the Faculty of Natural Science, Norwegian University of Science and Technology, for a scholarship to K. R. K.

Appendix A. Correction factor formulation

In this section, we derive a formulation of the flux-force relations for the composite membrane system that is based primarily on the transport coefficients of the bulk membrane and introduce correction terms that take interfacial contributions into account. We observe that

$$\left(\frac{1}{T_1^{s,m}}-\frac{1}{T_1^{s,l}}\right)+\left(\frac{1}{T_2^{s,l}}-\frac{1}{T_2^{s,m}}\right)=\left(\frac{1}{T_2^{s,l}}-\frac{1}{T_1^{s,l}}\right)-\left(\frac{1}{T_2^{s,m}}-\frac{1}{T_1^{s,m}}\right). \tag{A.1}$$

Furthermore, we have

$$\begin{aligned} J_u &= L_{uu}^{\mathrm{ms}}\Delta_{\mathrm{ms}}\frac{1}{T}-L_{um}^{\mathrm{ms}}\Delta_{\mathrm{ms}}\frac{\mu_w}{T},\\ J_w &= L_{mu}^{\mathrm{ms}}\Delta_{\mathrm{ms}}\frac{1}{T}-L_{mm}^{\mathrm{ms}}\Delta_{\mathrm{ms}}\frac{\mu_w}{T}, \end{aligned} \tag{A.2}$$

where the superscript ms on the conductances denotes the conductances of the composite system $\Gamma_1^s \oplus \Gamma_m \oplus \Gamma_2^s$ indicated in Fig. 1, and the differences $\Delta_{\mathrm{ms}} f = f_2^{s,l} - f_1^{s,l}$ for the arbitrary variable f. Then, inserting the flux-force relations for each of the two interface regions Γ_1^s and Γ_2^s into Eq. (A.1), inserting Eq. (A.2) for the fluxes, and rearranging, we obtain

$$\begin{aligned} \frac{1}{T_2^{s,m}}-\frac{1}{T_1^{s,m}} &= \mathscr{B}_{uu}\Delta_{\mathrm{ms}}\frac{1}{T}-\mathscr{B}_{um}\Delta_{\mathrm{ms}}\frac{\mu_w}{T}\\ -\left(\frac{\mu_{w,2}^{s,m}}{T_2^{s,m}}-\frac{\mu_{w,1}^{s,m}}{T_1^{s,m}}\right) &= \mathscr{B}_{mu}\Delta_{\mathrm{ms}}\frac{1}{T}-\mathscr{B}_{mm}\Delta_{\mathrm{ms}}\frac{\mu_w}{T} \end{aligned} \tag{A.3}$$

with

$$\begin{aligned} \mathscr{B}_{uu} &= 1-\left(R_{uu}^{s,1}+R_{uu}^{s,2}\right)L_{uu}^{\mathrm{ms}}-\left(R_{um}^{s,1}+R_{um}^{s,2}\right)L_{mu}^{\mathrm{ms}}\\ \mathscr{B}_{um} &= -\left(R_{uu}^{s,1}+R_{uu}^{s,2}\right)L_{um}^{\mathrm{ms}}-\left(R_{um}^{s,1}+R_{um}^{s,2}\right)L_{mm}^{\mathrm{ms}}\\ \mathscr{B}_{mu} &= -\left(R_{mu}^{s,1}+R_{mu}^{s,2}\right)L_{uu}^{\mathrm{ms}}-\left(R_{mm}^{s,1}+R_{mm}^{s,2}\right)L_{mu}^{\mathrm{ms}}\\ \mathscr{B}_{mm} &= 1-\left(R_{mu}^{s,1}+R_{mu}^{s,2}\right)L_{um}^{\mathrm{ms}}-\left(R_{mm}^{s,1}+R_{mm}^{s,2}\right)L_{mm}^{\mathrm{ms}}. \end{aligned} \tag{A.4}$$

If coupling effects are neglected, then $\mathscr{B}_{um}=0$, $\mathscr{B}_{mu}=0$, and $\mathscr{B}_{ii}=1-\left(R_{ii}^{s,1}+R_{ii}^{s,2}\right)/R_{ii}^{\mathrm{ms}}$, which recovers the simple electrical resistance analogy for heat and mass transfer. If the interfacial resistances are negligible compared to the resistances of the bulk membrane, then the driving forces across the composite system $\Gamma_1^s \oplus \Gamma_m \oplus \Gamma_2^s$ are the same across the bulk membrane Γ_m by itself, which is a typical situation assumed in the literature. Having

expressed the bulk driving forces as thermodynamically consistent linear combinations of the total driving forces over $\Gamma_1^s \oplus \Gamma_m \oplus \Gamma_2^s$, we rewrite the bulk flux-force equations in terms of the driving forces

$$\begin{aligned} J_u &= \frac{\ell^{\bar{m}}_{uu}\mathscr{B}_{uu} + \ell^{\bar{m}}_{um}\mathscr{B}_{mu}}{\delta}\Delta_{\mathrm{ms}}\frac{1}{T} - \frac{\ell^{\bar{m}}_{um}\mathscr{B}_{mm} + \ell^{\bar{m}}_{uu}\mathscr{B}_{um}}{\delta}\Delta_{\mathrm{ms}}\frac{\mu_w}{T} \\ J_w &= \frac{\ell^{\bar{m}}_{mu}\mathscr{B}_{uu} + \ell^{\bar{m}}_{mm}\mathscr{B}_{mu}}{\delta}\Delta_{\mathrm{ms}}\frac{1}{T} - \frac{\ell^{\bar{m}}_{mm}\mathscr{B}_{mm} + \ell^{\bar{m}}_{mu}\mathscr{B}_{um}}{\delta}\Delta_{\mathrm{ms}}\frac{\mu_w}{T}. \end{aligned} \tag{51}$$

From these expressions, one may derive the transport quantities that pertain to the system $\Gamma_1^s \oplus \Gamma_m \oplus \Gamma_2^s$, in terms of the bulk properties and the $\mathscr{B}_{ij}$ terms.

Appendix B. Iterative method for nonlinear effects

While the first approximations to the overall conductivities of the membrane system do incorporate some of the nonlinear effects present in the system due to the differing thermodynamic states of the two interfaces, the approximation is obtained by assuming constant values of the bulk resistivities throughout the bulk membrane. Since the resistivities do depend on the local thermodynamic state of the representative elementary volume element at a particular location along the axis of transport, we can expect nonlinear effects to occur also across the bulk of the membrane. In order to assess these effects, we demonstrate the iterative method for improving the accuracy of the predicted thermo-osmotic coefficient, as well as the temperature and pressure profiles in the bulk membrane. We define the coefficients

$$\begin{aligned} \mathscr{A}_{uu,i} &= R^{s,i}_{uu}L^{\mathrm{tot}}_{uu} + R^{s,i}_{um}L^{\mathrm{tot}}_{mu} \\ \mathscr{A}_{um,i} &= R^{s,i}_{uu}L^{\mathrm{tot}}_{mu} + R^{s,i}_{um}L^{\mathrm{tot}}_{mm} \\ \mathscr{A}_{mu,i} &= R^{s,i}_{mu}L^{\mathrm{tot}}_{uu} + R^{s,i}_{mm}L^{\mathrm{tot}}_{mu} \\ \mathscr{A}_{mm,i} &= R^{s,i}_{mu}L^{\mathrm{tot}}_{mu} + R^{s,i}_{mm}L^{\mathrm{tot}}_{mm} \end{aligned} \tag{B.1}$$

such that, for instance

$$\begin{aligned} \frac{1}{T_1^{s,m}} - \frac{1}{T_1^{s,l}} &= \mathscr{A}_{uu,1}\Delta_{1,2}\frac{1}{T} - \mathscr{A}_{um,1}\Delta_{1,2}\frac{\mu_w}{T}, \\ -\left(\frac{\mu_{w,1}^{s,m}}{T_1^{s,m}} - \frac{\mu_{w,1}^{s,l}}{T_1^{s,l}}\right) &= \mathscr{A}_{mu,1}\Delta_{1,2}\frac{1}{T} - \mathscr{A}_{mm,1}\Delta_{1,2}\frac{\mu_w}{T}. \end{aligned} \tag{B.2}$$

We can then solve for state variables inside the membrane close to the interface

$$\begin{aligned} \frac{1}{T_1^{s,m}} &= \frac{1}{T_1^{s,l}} + \mathscr{A}'_{uu,1}\Delta_{1,2}\frac{1}{T} + \mathscr{A}_{um,1}\left(\nu M_w R\Gamma_s\Delta_{1,2}m_s - \frac{V_w}{\bar{T}}\Delta_{1,2}p\right) \\ p_{w,1}^{s,m} &= \frac{T_1^{s,m}}{T_1^{s,l}}p_{w,1}^{\mathrm{sat}}\left(T_1^{s,l}, m_1\right)\exp\left(\mathscr{A}'_{mm,1}\left(\frac{V_w}{R\bar{T}}\Delta_{1,2}p - \nu M_w\Gamma_s\Delta_{1,2}m_s\right) - \mathscr{A}'_{mu,1}\Delta_{1,2}\frac{1}{RT}\right) \end{aligned} \tag{B.3}$$

where

$$\begin{aligned} \mathscr{A}'_{uu,1} &= \mathscr{A}_{uu,1} - H_{w,l}\mathscr{A}_{um,1} \\ \mathscr{A}'_{mu,1} &= \mathscr{A}_{mu,1} + H_{w,g}(T_1^{s,m})\mathscr{A}_{uu,1} - H_{w,l}\left(\mathscr{A}_{mm,1} + H_{w,g}(T_1^{s,m})\mathscr{A}_{um,1}\right) \\ \mathscr{A}'_{mm,1} &= \mathscr{A}_{mm,1} + H_{w,g}(T_1^{s,m})\mathscr{A}_{um,1} \end{aligned} \tag{B.4}$$

and the other interface obeys similar relations with the subscripts 1 replaced by 2. Computing the temperature $T_1^{s,m}$ inside the membrane then allows computation of the exponential factor that determines the departure of the actual vapor pressure near the interface from that of vapor in equilibrium with the interface, denoted $p_{w,1}^{\mathrm{sat}}\left(T_1^{s,l}, m_1\right)$. These values are then the first approximations to the actual boundary values of p_w and T inside the bulk of the membrane. To compute the actual profiles, we can take into account the dependence of the local resistivities on the local values of p_w and T by using the flux-force relations

$$\begin{aligned} \partial_x T &= -T^2 r^b_{uu}J_u - T^2 r^b_{um}J_w \\ -R\partial_x \ln p_w &= \left[r^b_{mu} + H_{w,g}r^b_{uu}\right]J_u + \left[r^b_{mm} + H_{w,g}r^b_{um}\right]J_w \end{aligned} \tag{B.5}$$

where the first approximations to the steady-state values of J_u and J_w are obtained through the first approximations to L_{ij}^{tot}. Solving these equations gives a first approximation to the actual profiles of T and p_w throughout the membrane. This can be used to obtain a better approximation of the total bulk resistances through numerical integration, which again a better approximation for L_{ij}^{tot} and more accurate values of J_u and J_w. This algorithm is repeated until an acceptable degree of accuracy is achieved.

Appendix C. Numerical expressions for transport properties

In order to use the theory presented, we require explicit expressions for the transport properties in terms of the state variables and the structural and chemical properties of the membrane system. To construct the bulk resistances, we need the pore resistances obtained by inserting Eq. (12) into Eq. (8). The transport properties of the pore are obtained from the generalized Bosanquet formula (Eq. (11)) when the resistivities in the limits Kn→0 and Kn→∞ are known. We provide in the following the expressions for the transport properties in these two limits. In the limit Kn→∞, we have

$$\begin{aligned} D_{\mathrm{K}} &= \frac{8a}{3}\sqrt{\frac{RT}{2\pi M_w}}\mathscr{K}_{\mu\mu}, \\ \lambda_{\mathrm{K}} &= \frac{2pD_{\mathrm{K}}}{T}\left[x_w\mathscr{K}_{qq} + (1-x_w)\sqrt{\frac{M_w}{M_a}}\right], \\ Q^*_{\mathrm{K}} &= H_{w,g} - \frac{RT}{2}\frac{\mathscr{K}_{q\mu}}{\mathscr{K}_{\mu\mu}} = H_{w,g} + q^*_{\mathrm{K}}, \end{aligned} \tag{C.1}$$

where a is the cylinder radius, M_w is the water molar mass, M_a the averaged molar mass of air, x_w and $H_{w,g}$ the mole fraction and molar enthalpy of water vapor, and the coefficients $\mathscr{K}_{ij}$ are correction factors accounting for the particle-wall interaction, where further details can be found in Ref. [21].

The limit Kn→0 is simply the case of a bulk mixture of water vapor and air. We require the interdiffusion coefficient, the heat of transfer, and the thermal conductivity. The interdiffusion coefficient can be expressed with the correlation (in units m^2/s) [35].

$$D_h = 1.895\cdot 10^{-5}\frac{T^{2.072}}{p}. \tag{C.2}$$

We calculate the energy of transfer with the approximate formula derived in Appendix D

$$Q^*_h = H_{w,g} - \frac{0.072(1-x_w)RT}{x_w^2 + 1.228(1-x_w)} = H_{w,g} + q^*_h. \tag{C.3}$$

The thermal conductivity of humid air can be expressed by the semi-empirical formula based on expressions for gas mixtures in kinetic theory [36].

$$\lambda_h = \frac{\lambda_w x_w}{x_w + \alpha_{wa}(1-x_w)} + \frac{\lambda_a(1-x_w)}{1 + x_w(\alpha_{aw}-1)} \tag{C.4}$$

where α_{wa} and α_{aw} are used as fitting parameters based on mixture data given correlations for the thermal conductivities λ_w and λ_a of pure water vapor and dry air, respectively. Based on data from [37], we obtain the values $\alpha_{wa} = 1.167$ and $\alpha_{aw} = 0.886$.

The values of the interface resistances R^{gl}_{ij} were tabulated as functions of temperature. To 1% accuracy, we find that the values in Ref. [24] satisfy

$$\ln\left(\frac{R^{\mathrm{gl}}_{ij}}{R^{\mathrm{gl}}_{ij,0}}\right) = a_1\frac{T}{T_0} + a_2\left(\frac{T}{T_0}\right)^2, \tag{C.5}$$

where T refers to the liquid temperature and $T_0 = 300$ K. The least-squares fit values of the coefficients can be found in Table C.1. The reference values are $R^{\mathrm{gl}}_{qq,0} = 1.7076\cdot 10^{-7}\ \mathrm{m^2\ W^{-1}\ K^{-1}}$, $R^{\mathrm{gl}}_{q\mu,0} = 1.1085\cdot 10^{-4}\ \mathrm{m^2\ s\ mol^{-1}\ K^{-1}}$ and $R^{\mathrm{gl}}_{\mu\mu,0} = 9.3350\cdot 10^{-2}\ \mathrm{J\ s\ m^2\ K^{-1}\ mol^{-2}}$.

Table C.1
Parameters for the interpolation formula in Eq. (C.5) for the resistivities of the plane vapor-liquid interface, fitted to data tabulated in [24].

	a_1	a_2
R^{gl}_{qq}	11.252	−11.815
$R^{\mathrm{gl}}_{q\mu}$	11.935	−11.432
$R^{\mathrm{gl}}_{\mu\mu}$	12.701	−10.974

The coupling coefficients as well as the interfacial resistances are routinely neglected in the MD literature [3], while the bulk diffusion coefficient D_m and the bulk thermal conductivity λ_m have been studied in detail. The thermal conductivity is furthermore taken to be some combination of the thermal conductivity of humid air and that of the solid membrane material, of which a thorough assessment can be found in [31].

As for the liquid-solid thermal resistance R^{ls}_{qq}: A molecular dynamics investigation by Xue et al. [38] revealed that for a non-wetting liquid-solid interaction, the thermal resistance depends exponentially on the wetting parameter commonly applied with Lennard-Jones potentials. An experimentally verified correlation between the contact angle and the thermal conductance was proposed by Shenogina et al. [39], and in terms of our notation, it reads

$$\frac{1}{R^{ls}_{qq}} = T^2 B(1+\cos(\theta_e)), \tag{C.6}$$

with the factor $B = 85\ \mathrm{MW\ m^{-2}\ K^{-1}}$. This means that R^{ls}_{qq} is on the order of $10^{-13}\ \mathrm{m^2\ W^{-1}\ K^{-1}}$, which is 5–6 orders of magnitude smaller than that of the vapor-liquid interface. This demonstrates that the degree of liquid-solid contact is important when considering the question of whether or not the interfacial thermal resistance may be neglected.

Appendix D. Heat of transfer in the bulk gas mixture

The best-studied quantity relating to heat-mass coupling in gas mixtures by the kinetic theory community is the thermal diffusion factor α_T, which can be expressed in terms of the heat of transfer q_h^* as $\alpha_T = q_h^*/RT(1-x_w)$. It was demonstrated by Laranjeira [40] that α_T^{-1} is proportional to the mole fractions of the mixture components. In accordance with the work by Mason and Smith [41], we may express the composition dependence as

$$\frac{1}{\alpha_T} = \frac{x_w}{\alpha_T^v} + \frac{1-x_w}{\alpha_T^a}, \tag{D.1}$$

where the quantities α_T^v and α_T^a can be approximated with a lorentzian and a quasi-lorentzian model, respectively. In more recent work by Mason, Kihara's method was applied to obtain explicit expressions [42]

$$\alpha_T^v = \frac{1}{x_w}\left[2 - \left(\frac{\partial \ln D_h}{\partial \ln T}\right)_p\right], \quad \alpha_T^a = \frac{3x_w\eta_w RT}{2M_w p D_h}\alpha_T^v, \tag{D.2}$$

where η_w is the dynamic shear viscosity of pure water vapor. We see that the sign is determined by the temperature dependence of the interdiffusion coefficient. Since D_h in Eq. (C.2) varies with temperature to a power greater than 2, $\alpha_T < 0$, as expected by kinetic arguments based on water being the lighter component in the mixture. The viscosity of water vapor was measured by several workers, and compiled together in [43], from which a power law fit gives the correlation (in units Pa s)

$$\eta_w = 1.935\cdot 10^{-8} T^{1.097}. \tag{D.3}$$

We note that $T\eta_w \propto T^{2.097}$, which is very close to the temperature dependence of pD_h. The ratio $T\eta_w/pD_h$ makes up the temperature dependence of α_T^a which is then close to negligible. We find a simple formula

$$\frac{q_h^*}{RT} = \frac{-0.072(1-x_w)}{x_w^2 + 1.415\cdot T^{-1/40}(1-x_w)}, \tag{D.4}$$

which vanishes for pure water vapor, and q_h^* ranges between −130 and − 180 J mol^{-1} at infinite dilution in air between 273 K and 373 K.

References

[1] C. Forman, I.K. Muritala, R. Pardemann, B. Meyer, Estimating the global waste heat potential, Renew. Sust. Energ. Rev. 57 (2016) 1568–1579, https://doi.org/10.1016/j.rser.2015.12.192.

[2] S. Postel, The Last Oasis, Taylor & Francis Group, 1992.

[3] M. Khayet, T. Matsuura, Membrane Distillation: Principles and Applications, Elsevier, 2011.

[4] S. Soukane, H.S. Son, M. Mustakeem, M. Obaid, A. Alpatova, A. Qamar, Y. Jin, N. Ghaffour, Materials for energy conversion in membrane distillation localized heating: review, analysis and future perspectives of a paradigm shift, Renew. Sust. Energ. Rev. 167 (2022), 112702.

[5] H. Julian, N. Nurgirisia, G. Qiu, Y.-P. Ting, I.G. Wenten, Membrane distillation for wastewater treatment: current trends, challenges and prospects of dense membrane distillation, J. Water Process Eng (2022) 102615.

[6] A. Alkhudhiri, N. Darwish, N. Hilal, Membrane distillation: A comprehensive review, Desalination (2012) 2–18.

[7] J.P.G. Villaluenga, S. Kjelstrup, A non-equilibrium thermodynamics model of multicomponent mass and heat transport in pervaporation processes, J. Non-Equilib. Thermodyn. 37 (2012) 353–376.

[8] D. Bedeaux, S. Kjelstrup, Irreversible thermodynamics—a tool to describe phase transitions far from global equilibrium, Chem. Eng. Sci. 59 (2004) 109–118.

[9] R.W. Schofield, A.G. Fane, C.J.D. Fell, Gas and vapour transport through microporous membranes. II. Membrane distillation, J. Membr. Sci. 53 (1990) 173–185, https://doi.org/10.1016/0376-7388(90)80012-B.

[10] N. Kuipers, J.H. Hanemaaijer, H. Brouwer, J. van Medevoort, A. Jansen, F. Altena, P. van der Vleuten, H. Bak, Simultaneous production of high-quality water and electrical power from aqueous feedstock's and waste heat by high-pressure membrane distillation, Desalin. Water Treat. 55 (2014) 2766–2776, https://doi.org/10.1080/19443994.2014.946724.

[11] W.A. Phillip, Thermal-energy conversion: under pressure, *Nat.* Energy 1 (2016) 16101.

[12] A.P. Straub, N.Y. Yip, S. Lin, J. Lee, M. Elimelech, Harvesting low-grade heat energy using thermo-osmotic vapour transport through nanoporous membranes, Nat. Energy 1 (2016) 16090.

[13] K. Park, D.Y. Kim, D.R. Yang, Theoretical analysis of pressure retarded membrane distillation (prmd) process for simultaneous production of water and electricity, Ind. Eng. Chem. Res. 56 (2017) 14888–14901.

[14] F. Mahmoudi, G.M. Goodarzi, S. Dehghani, A. Akbarzadeh, Experimental and theoretical study of a lab scale permeate gap membrane distillation setup for desalination, Desalination 419 (2017) 197–210.

[15] F. Mahmoudi, A. Date, A. Akbarzadeh, Further investigation of simultaneous fresh water production and power generation concept by permeate gap membrane distillation system, J. Membr. Sci. 572 (2019) 230–245, https://doi.org/10.1016/j.memsci.2018.11.004.

[16] M.T. Rauter, S.K. Schnell, S. Kjelstrup, Cassie-Baxter and Wenzel states and the effect of interfaces on transport properties across membranes, J. Phys. Chem. B 125 (2021) 12730–12740.

[17] S. Kjelstrup, D. Bedeaux, Non-Equilibrium Thermodynamics of Heterogeneous Systems, World Scientific, 2008.

[18] C. H. Bosanquet. BR-507. British TA Report, 1944.

[19] W.G. Pollard, R.D. Present, On gaseous self-diffusion in long capillary tubes, Phys. Rev. 73 (1948) 762–772.

[20] R. Krishna, J.M. van Baten, Investigating the validity of the Bosanquet formula for estimation of diffusivities in mesopores, Chem. Eng. Sci. 69 (2012) 684–688.

[21] K.R. Kristiansen, S. Kjelstrup, Particle flow through a hydrophobic nanopore: effect of long-ranged wall-fluid repulsion on transport coefficients, Phys. Fluids 33 (2021), 102001, https://doi.org/10.1063/5.0066433.

[22] R.N. Wenzel, Resistance of solid surfaces to wetting by water, Ind. Eng. Chem. 28 (1936) 988–994.

[23] A.B.D. Cassie, S. Baxter, Wettability of porous surfaces, Trans. Faraday Soc. 40 (1944) 546–551.

[24] Ø. Wilhelmsen, T.T. Trinh, A. Lervik, V.K. Badam, S. Kjelstrup, D. Bedeaux, A coherent description of transport across the water interface: from nanodroplets to climate models, Phys. Rev. E 93 (2015), 032801.

[25] M.T. Rauter, A. Aasen, S. Kjelstrup, Ø. Wilhelmsen, A comparative study of experiments and theories on steady-state evaporation of water, Chem. Thermodyn. Thermal Anal. 8 (2022), 100091.

[26] J. Liu, Q. Wang, H. Shan, H. Guo, B. Li, Surface hydrophobicity based heat and mass transfer mechanism in membrane distillation, J. Membr. Sci. 580 (2019) 275–288.

[27] Ø. Wilhelmsen, T.T. Trinh, S. Kjelstrup, T.S. van Erp, D. Bedeaux, Heat and mass transfer across interfaces in complex nanogeometries, Phys. Rev. Lett. 114 (6) (2015), 065901.

[28] Y.A. Cengel, Heat and Mass Transfer - A Practical Approach, McGraw-Hill, 2006.

[29] M. Khayet, A.O. Imdakm, T. Matsuura, Monte Carlo simulation and experimental heat and mass transfer in direct contact membrane distillation, Int. J. Heat Mass Transf. 53 (2010) 1249–1259, https://doi.org/10.1016/j.ijheatmasstransfer.2009.12.043.

[30] M. Khayet, J.I. Mengual, G. Zakrzewska-Trznadel, Direct contact membrane distillation for nuclear desalination. Part i: review of membranes used in membrane distillation and methods for their characterisation, Int. J. Nuclear Desalination 1 (2005).

[31] M.C. Garc'ıa-Payo, M.A. Izquierdo-Gil, Thermal resistance technique for measuring the thermal conductivity of thin microporous membranes, J. Phys. D 37 (2004) 3008.

[32] M.C. García-Payo, M.A. Izquierdo-Gil, C. Fernández-Pineda, Wetting study of hydrophobic membranes via liquid entry pressure measurements with aqueous alcohol solutions, J. Colloid Interface Sci. 15 (2000) 420–431, https://doi.org/10.1006/jcis.2000.7106.

[33] Ø. Wilhelmsen, D. Reguera, Evaluation of finite-size effects in cavitation and droplet formation, J. Chem. Phys. 142 (2015), 064703.
[34] Ø. Wilhelmsen, D. Bedeaux, S. Kjelstrup, D. Reguera, Communication: Superstabilization of fluids in nanocontainers, J. Chem. Phys. 141 (7) (2014), 071103.
[35] J. Phattaranawik, R. Jiraratananon, Effect of pore size distribution and air flux on mass transport in direct contact membrane distillation, J. Membr. Sci. 215 (2003) 75–85, https://doi.org/10.1016/S0376-7388(02)00603-8.
[36] S. Chapman, T.G. Cowling, The Mathematical Theory of Non-Uniform Gases, Cambridge University Press, 1970.
[37] P.T. Tsilingiris, Thermophysical and transport properties of humid air at temperature range between 0 and 100°C, Energy Convers. 49 (2008) 1098–1110.
[38] L. Xue, P. Keblinski, S.R. Phillpot, et al., Two regimes of thermal resistance at a liquid-solid interface, J. Chem. Phys. 118 (2003) 337.
[39] N. Shenogina, R. Godawat, P. Keblinski, S. Garde, How wetting and adhesion affect thermal conductance of a range of hydrophobic to hydrophilic aqueous interfaces, Phys. Rev. Lett. 102 (2009), 156101.
[40] M.F. Laranjeira, An elementary theory of thermal and pressure diffusion in gaseous binary and complex mixtures II. binary mixtures with experimental comparison, Physica 26 (1960) 417–430, 655 656 657 658 659 660 661 662.
[41] E.A. Mason, F.J. Smith, Thermal diffusion in almost Lorentzian mixtures, J. Chem. Phys. 44 (1966) 3100.
[42] E.A. Mason, Higher approximations for the transport properties of binary gas mixtures. II. Applications, *J. Chem. Phys*. 27 (2004) 782, https://doi.org/10.1063/1.1743829.
[43] C.J. Smith, An experimental study of the viscous properties of water vapour, Proc. R. Soc. Lond. 106 (1924), https://doi.org/10.1098/rspa.1924.0056.